

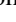

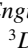


Pseudospectral Landau-Lifshitz description of magnetization dynamicsKyle Rockwell ¹, Joel Hirst ², Thomas A. Ostler ³ and Ezio Iacocca ¹¹*Center for Magnetism and Magnetic Nanostructures, University of Colorado Colorado Springs, Colorado Springs, Colorado 80918, USA*²*Materials and Engineering Research Institute, Sheffield Hallam University, Howard Street, Sheffield S1 1WB 22, United Kingdom*³*Department of Physics and Mathematics, University of Hull, Hull HU6 7RX, United Kingdom* (Received 21 December 2023; revised 17 April 2024; accepted 30 April 2024; published 9 May 2024)

Magnetic materials host a wealth of nonlinear dynamics, textures, and topological defects. This is possible due to the competition between strong nonlinearity and dispersion, which act at the atomic scale, as well as long-range interactions. However, these features are difficult to study analytically and numerically because of the vastly different temporal and spatial scales involved. Here, we present a pseudospectral approach for the Landau-Lifshitz equation that invokes energy and momentum conservation embodied in the magnon dispersion relation to accurately describe both atomic and continuum limits. Furthermore, this approach enables analytical study at every scale. We show the applicability of this model in both the continuum and atomic limit by investigating modulational instability and ultrafast evolution of magnetization due to transient grating, respectively, in a one-dimensional ferromagnetic chain with perpendicular magnetic anisotropy. This model provides the possibility of grid-independent multiscale numerical approaches that will enable the description of singularities within a single framework.

DOI: [10.1103/PhysRevB.109.L180404](https://doi.org/10.1103/PhysRevB.109.L180404)

Nonlinear and far-from-equilibrium dynamics give rise to fascinating physics because of novel phenomena [1–3] and their potential applications [4,5]. Magnetic materials are fundamentally interesting to study from this perspective because their nonlinearity and dispersion give rise to a wealth of local and nonlocal defects [6–12] as well as, e.g., symmetry-dependent domain-wall rearrangement [13–15], ultrafast domain-wall speeds [16], and stabilization of topological phases [17,18].

From a theoretical and numerical point of view, investigation of such dynamics presents many challenges. For example, solitons typically exhibit a singularity at their core, which requires atomic scale resolution, while their environment is relatively smooth [11,19]. In addition, in far-from-equilibrium phenomena, both short- and long-range effects play a role at picosecond timescales [17]. There are traditionally two approaches to resolve the dynamics. On the one hand, atomistic spin dynamics (ASD) [20–25] takes into account a discrete Heisenberg Hamiltonian to resolve the interactions between atomic magnetic moments. On the other hand, micromagnetic simulations [26,27] are based on the series expansion of the Heisenberg Hamiltonian in a continuum regime [28], which can resolve domain structures. Because of the series expansion of the exchange interaction, there is a spatiotemporal transition region that is poorly described by either method, limiting the understanding of several problems of current interest, such as the stabilization of topological solitons or domains by ultrafast excitation, and the conditions to nucleate and stabilize three-dimensional solitons [11,29].

Here, we introduce a pseudospectral Landau-Lifshitz (PS-LL) equation that closes the gap between ASD and micromagnetic simulations. In contrast to previous multiscale approaches that link ASD and micromagnetic simulations,

e.g., Refs. [19,30–32], we seek a description that targets the transition region. Our fundamental assumption is that there must be continuity in both energy and momentum, which we enforce by ensuring a proper description of the dispersion relation of magnons, the quanta of angular momentum, across scales. This goal is achieved in Fourier space, and it is similar to the “dispersion engineering” approach introduced by Whitham in the context of fluid dynamics [33]. In addition, working in Fourier space enables both grid independence as well as analytical study of atomic scale and micrometer scale effects on an equal footing, thus providing a formalism to investigate nonlinear textures.

While the PS-LL model is general, we focus here on its description and implementation for a one-dimensional (1D) ferromagnetic chain with perpendicular magnetic anisotropy. First, we demonstrate that the magnon dispersion relation is numerically reproduced and that the computation is grid-independent. Second, we show that modulational instability [34] is numerically reproduced, agreeing with analytical expressions obtained through a spin hydrodynamic representation [35–38]. Third, we consider ultrafast transient grating [39–43] as a test case to compare ASD and PS-LL, demonstrating excellent agreement in the energy evolution between both models. Because of the arbitrary resolution in space, the PS-LL model is ideal to investigate topological textures and far-from-equilibrium dynamics. The generality of the model also suggests further refinement by integration with existing micromagnetic approaches, multigrid expansions, and multisublattice systems.

The discrepancy in energy and momentum space between ASD and the micromagnetic approach is especially apparent in the magnon dispersion relation. For example, the magnon dispersion relation for 1D ferromagnets with nearest-neighbor interactions can be obtained from the discrete Heisenberg

Hamiltonian

$$\omega(k) = \gamma\mu_0 M_s \frac{2D}{a^2\hbar} [1 - \cos(ka)], \quad (1)$$

where γ is the gyromagnetic ratio, μ_0 is the vacuum permeability, M_s is the saturation magnetization, D is the exchange stiffness, \hbar is the reduced Planck's constant, and a is the lattice constant of the crystal. Upon first-order Taylor expansion, the dispersion relation reduces to the well-known k^2 form obtained in the micromagnetic limit,

$$\omega(k) \approx \gamma\mu_0 M_s \frac{D}{\hbar} k^2 = \gamma\mu_0 M_s \lambda_{\text{ex}}^2 k^2, \quad (2)$$

where we define the exchange length $\lambda_{\text{ex}} = \sqrt{D/\hbar}$. In this limit, the energy of magnons at the first Brillouin zone (FBZ) boundary is a factor $\pi^2/4 \approx 2.46$ larger than in ASD. More dramatically, the group velocity of magnons is substantially different, being exactly zero for the discrete Heisenberg Hamiltonian and $\gamma\mu_0 M_s D\pi^2/(\hbar a^2)$ in the micromagnetic limit. This implies that small features, such as topological defects, are difficult to stabilize in micromagnetic simulations.

A similar problem was encountered in the description of shallow water waves, where the Korteweg–de Vries (KdV) equation is a long-wave approximation of the Euler equations [44]. In his seminal work, Whitham [33] proposed a mathematical solution whereby the term giving rise to wave dispersion in the KdV equation, u_{xxx} , could be modified to exactly reproduce the phase velocity obtained from Euler equations. For this, a kernel κ was introduced so that $u_{xxx} \rightarrow \kappa * u_x$, where $*$ represents convolution. Because of the convolution theorem, this approach is numerically apt for spectral methods.

In the context of ferromagnets, the magnetization dynamics are described by the Landau-Lifshitz-Gilbert (LLG) equation. In the case in which $\alpha \ll 1$, the LLG equation can be approximated to a Landau-Lifshitz (LL) form, which has the benefit of being an implicit equation. We introduce the PS-LL equation

$$\begin{aligned} \frac{\partial \mathbf{m}}{\partial t} = & -\mathbf{m} \times [(\gamma\mu_0 M_{\text{eff}} \mathbf{h}_l - \mathcal{F}^{-1}\{\omega(k) \hat{\mathbf{m}}\}) \\ & + \alpha \mathbf{m} \times \mathbf{m} \times (\gamma\mu_0 M_{\text{eff}} \mathbf{h}_l - \mathcal{F}^{-1}\{\omega(k) \hat{\mathbf{m}}\})], \quad (3) \end{aligned}$$

where \mathbf{m} is the magnetization vector normalized to the saturation magnetization, M_s , and \mathbf{h}_l contains the local fields normalized to the effective magnetization $M_{\text{eff}} = |H_k - M_s|$, where H_k is the uniaxial anisotropy field [37]. The exchange field and long-range interactions are described in Fourier space as $\omega(k)\hat{\mathbf{m}}$, where $\omega(k)$ is the desired dispersion relation. In Eq. (3), $\mathcal{F}^{-1}\{\cdot\}$ represents the inverse Fourier transform, indicating that the dispersion relation is used as a convolution kernel. This is different from the approach introduced by Whitham [33], which focused on describing the phase velocity rather than the dispersion relation.

The PS-LL is generally stated in Eq. (3), but here we simplify the analysis to the case of a 1D chain subject to a normalized external field h_o and perpendicular magnetic anisotropy (PMA), both normal to the plane, $\mathbf{h}_l = (h_o + m_z)\hat{z}$, and exchange interaction. A nonlocal dipole field is not included here to focus on the correct description of the exchange interaction. It can be readily shown that the magnon dispersion

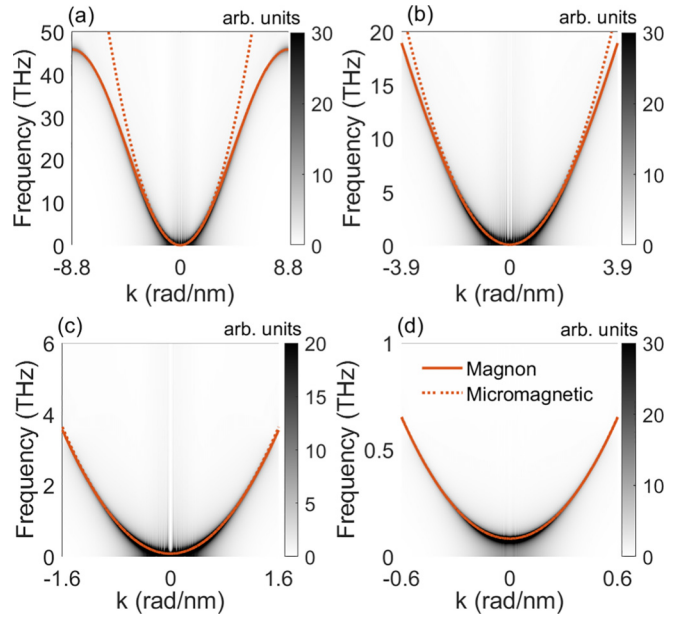


FIG. 1. Dispersion relation from PS-LL in a 1D ferromagnetic chain. The cells are set to (a) $a = 0.355$ nm, (b) 0.8 nm, (c) 2 nm, and (d) 5 nm. The analytical magnon dispersion relation is overlaid with solid red curves and the micromagnetic approximation with red dashed curves. In all cases, the PS-LL reproduces the magnon dispersion relation up to the highest resolved wave number.

relation $\omega(k)$ is directly recovered from Eq. (3) by imposing the plane-wave solution $m_z \approx 1$ and $m_x, m_y \propto e^{i(kx - \omega t)}$. A detailed derivation is provided in the Supplemental Material SI 1 [45].

The numerical implementation of PS-LL also reproduces the correct dispersion relation, shown in Fig. 1(a). For this numerical solution, we set parameters for CoFe/Ni, e.g., Ref. [15]: $M_s = 770$ kA/m, $H_k = 1550$ kA/m, $\lambda_{\text{ex}} = 7.3$ nm, and lattice constant $a \approx 0.355$ nm. The 1D ferromagnetic chain has an equilibrium orientation along the m_z component. We introduce a δ -like defect in the center of the chain, so that $m_x = 1$ and $m_z = 0$ at that point. The evolution of this defect results in outward propagating waves [46] that access all available magnons in the FBZ. To resolve the highest energy magnons in the FBZ, we employ an ode45 solver modified to enforce $|\mathbf{m}| = 1$ at every iteration step. The simulation is evolved for 10 ps and the solutions are sampled every 10 fs so that the maximally resolved frequency is 50 THz. The numerical result using an atomic cell size is shown in Fig. 1(a) with black contrast. We overlay the magnon dispersion relation by a solid red curve and the micromagnetic approximation by a red dashed curve, demonstrating that the PS-LL method correctly describes the magnon dispersion relation.

Because the PS-LL equation considers the dispersion relation within the FBZ, it is expected to be grid-independent and smoothly approach the micromagnetic approximation. We verify these statements by investigating the model's dependence on computational cell size. The calculations of the magnon spectra are shown in Fig. 1 for cell sizes of (b) 0.8 nm, (c) 2 nm, and (d) 5 nm. In all these cases, we find excellent agreement between the calculation and the magnon dispersion in the ranges of wave numbers corresponding to each cell size.

In particular, the PS-LL model agrees with the micromagnetic dispersion for sufficiently large cell sizes, i.e., panels (c) and (d). From these results, we conclude that the proposed PS-LL method is grid-independent and smoothly transitions to the micromagnetic approximation. It is worth noting that, as a pseudospectral method, the PS-LL can be used with cell sizes smaller than the lattice constant and thus resolve the dispersion past the FBZ. While this has limited physical application, it implies that the periodicity of the problem is respected. An example of a magnon dispersion relation for a cell size $0.2 \text{ nm} < a$ is shown in the Supplemental Material SI 2 [45].

The PS-LL also enables analytical investigation, insofar as solutions can be obtained in Fourier space. For example, it is possible to apply a spin hydrodynamic formulation [35–38] to the PS-LL, where we take advantage of the uniaxial symmetry of the local field to introduce a spin density $n = m_z$ and a fluid velocity $u = -\nabla\phi = -\nabla[\text{atan}(m_y/m_x)]$. This approach simplifies the description of chiral magnetization states and allows one to obtain the dispersion relation of magnons on such states. The full derivation is presented in the Supplemental Material SI 3 [45].

Here, we focus on the particular example of modulational instability (MI) [34]. In focusing media, the dispersion of waves on a fluid flow is complex for a range of wave numbers $0 < k < k_c$. This implies that random perturbations in that range tend to grow exponentially in magnitude. Magnetic materials with PMA are focusing media, and MI was demonstrated in the framework of the micromagnetic LL equation [37,38]. The same behavior is expected from the PS-LL equation since MI is active in the micromagnetic regime. For simplicity, we consider a uniform magnetization state, $u = 0$, and an average spin density \bar{n} . In this case, the dispersion relation from spin hydrodynamics simplifies to

$$\tilde{\omega}(k) = \pm\omega(k)\sqrt{1 - \frac{\gamma\mu_0 M_{\text{eff}}(1 - \bar{n}^2)}{\omega(k)}}, \quad (4)$$

which is valid for $0 \leq \bar{n} < 1$. Clearly, $\tilde{\omega}(k) \rightarrow \omega(k)$ when $\bar{n} \rightarrow 1$. MI occurs when the dispersion relation is complex. Therefore, we solve for the conditions leading to a negative argument in the square root of Eq. (4), $\omega(k) < \gamma\mu_0 M_{\text{eff}}(1 - \bar{n}^2)$. Solving for the equality leads to the cutoff wave number for MI,

$$k_c = \frac{1}{a} \arccos \left[1 - \frac{a^2 h_k (1 - \bar{n}^2)}{2\lambda_{\text{ex}}^2} \right]. \quad (5)$$

For the CoFe/Ni parameters used above, the cutoff wave number is $k_c = 0.19 \text{ rad nm}^{-1}$, which is equivalent to a wavelength of 33 nm that is well described in the micromagnetic approximation, as seen in Fig. 1(d). This confirms that MI is a long-wave phenomenon. Expanding the arccos in Eq. (5) leads to $\lambda_{\text{ex}}^2 k_c^2 = h_k(1 - \bar{n}^2)$, in agreement with the cutoff frequency derived from the micromagnetic LL equation [38]. The growth rate Γ is simply given by the imaginary part of Eq. (4) within the MI band. We show the growth rate for various values of \bar{n} in Fig. 2(a). We find growth rates on the order of tens of GHz, equivalent to time constants under 100 ps. k_c is reduced as $\bar{n} \rightarrow 1$, and MI is completely suppressed in the limit of $\bar{n} = 1$.

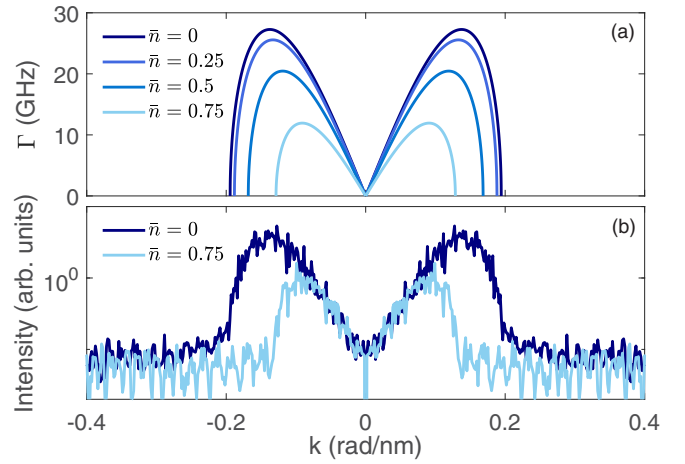


FIG. 2. (a) Calculation of the growth rate Γ for $\bar{n} = 0, 0.25, 0.5$, and 0.75 . As the PMA magnet is brought more into the plane, the MI band and maximum growth rate increase. (b) Spectrum of the m_z component after a $t = 50 \text{ ps}$ obtained by PS-LL. The simulation is initialized at a constant m_z and perturbed with a small, uniformly distributed noise. The spectra of 100 instances are averaged to minimize noise in the Fourier transform. Excellent agreement between the spectra and the growth rates is observed.

Because MI is a linear instability condition, it is possible to directly observe the growth rate from the numerical solution of the PS-LL. We set an initial condition $\bar{n} + \eta$, where η is random noise with uniform distribution and amplitude of 0.001. We evolve the simulation for 50 ps using a cell size equal to the lattice constant a . The spectrum of n is shown in Fig. 2(b) for $\bar{n} = 0$ and 0.75 , in excellent agreement with the growth rate and the cutoff wave number predicted by Eq. (5). For these results, we averaged the spectrum of 100 simulations to reduce noise. The observation of MI demonstrates that the PS-LL model can be used to analytically derive generalized spin hydrodynamic equations and that the model correctly describes wave phenomena captured by the micromagnetic approximation while maintaining stability due to large wave numbers.

We now investigate a regime in which ASD are required to correctly describe the magnetization dynamics. Ultrafast transient grating [39–43] is an experimental technique in which the phases of two femtosecond optical pulses are adjusted to produce a periodic profile on a material. The periodicity can be tuned from 10 nm to over 100 nm; this large range of wavelengths lies within the transition regime between ASD and micromagnetic simulations, making it a good test for the PS-LL model. ASD simulations are able to describe the dynamics, but at significant computational cost, whereas the micromagnetic description breaks down in this regime. To test the accuracy of PS-LL with respect to ASD and the micromagnetic approximation, we model a quasi-1D ferromagnetic nanowire of dimensions $400 \text{ nm} \times 1 \text{ nm} \times 1 \text{ nm}$ subject to periodic boundary conditions on the long axis. The nanowire is initialized with a periodic train of pulses of Gaussian profile that mimics transient grating. The number of pulses, N , is related to the Gaussian standard deviation, σ , such that $3N\sigma = 400 \text{ nm}$, the length of the nanowire. The magnetization under each pulse is then randomized to account

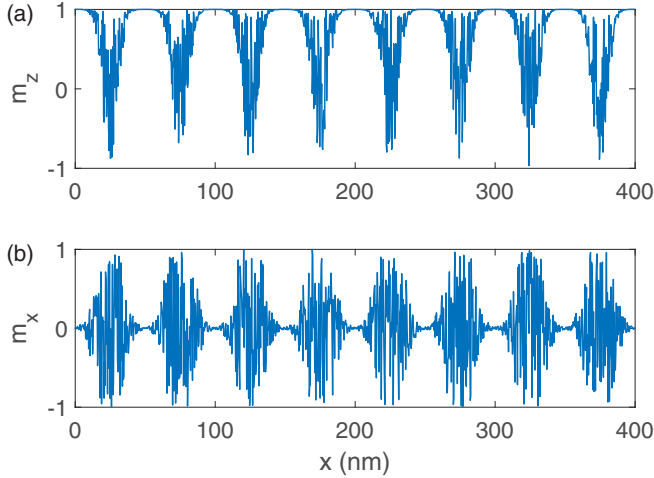


FIG. 3. Initial magnetization for a train of eight Gaussian pulses in the 1D ferromagnetic chain. (a) m_z component and (b) m_x component.

for the thermal origin of the distribution. In particular, we use uniform random distributions of the m_z component and the in-plane phase angle ϕ such that $m_x = \sqrt{1 - m_z^2} \cos(\phi)$ and $m_y = \sqrt{1 - m_z^2} \sin(\phi)$. An example of an initial condition with $N = 8$ is shown in Fig. 3 for the (a) m_z and (b) m_x components.

The initial magnetization state was simulated with ASD and PS-LL over a time span of 5 ps. Details on the implementation of ASD simulations are provided in the Supplemental Material SI 4 [45]. To unambiguously compare with the micromagnetic approximation, we implemented the following pseudospectral approach:

$$\frac{\partial \mathbf{m}}{\partial t} = -\mathbf{m} \times [(\gamma \mu_0 M_{\text{eff}} \mathbf{h}_1 - \mathcal{F}^{-1}\{k^2 \hat{\mathbf{m}}\}) + \alpha \mathbf{m} \times \mathbf{m} \times (\gamma \mu_0 M_{\text{eff}} \mathbf{h}_1 - \mathcal{F}^{-1}\{k^2 \hat{\mathbf{m}}\})]. \quad (6)$$

In this case, the kernel is the micromagnetic dispersion relation; this further demonstrates the generalizability of this method. We show that this approach reproduces the micromagnetic magnon dispersion in the Supplemental Material SI 5 [45].

To compare the methods, we compute the exchange energy as $E_{\text{ex}} = (Aa/2) \sum_i \mathbf{m}_i \cdot (\mathbf{m}_{i-1} + \mathbf{m}_{i+1})$. The results for an initial state with $N = 8$ pulses are shown in Fig. 4(a). The PS-LL, shown by a solid blue curve, shows a remarkable agreement with ASD, shown with hollow black circles. In contrast, the exchange energy in the micromagnetic approximation is minimized more rapidly during the first picosecond, due to the high energy of short waves and their concomitant large damping rate. The percentage energy error is shown in Fig. 4(b), where we note that the maximum error between the PS-LL and ASD $\approx 0.09\%$, in contrast to a maximum of $\approx 9.5\%$ for the micromagnetic approximation. These qualitative trends are maintained for other number of pulses. Results from 1 and 16 pulses are provided in the Supplemental Material SI 6 [45].

The energy discrepancy also has consequences in the evolution and recovery of the average magnetization. There

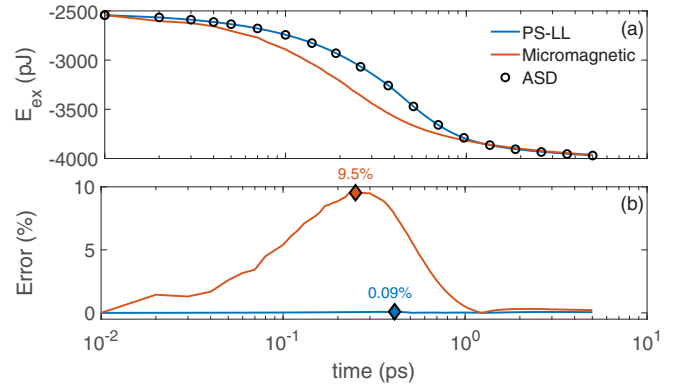


FIG. 4. (a) Comparison of the temporal evolution of exchange energy between PS-LL in the solid blue curve, micromagnetic approximation in the solid red curve, and ASD in hollow black circles. Excellent agreement with ASD is observed. The associated percentage error is shown in panel (b), with LLG topping at 9.5% vs PS-LL at 0.09%. The time is shown in a natural logarithmic scale.

is a notable difference between the group velocities predicted from the magnon dispersion and its micromagnetic approximation. In the former, $v_g = 2\gamma \mu_0 M_s (D/\hbar a) \sin(ka)$ while the micromagnetic approximation leads to $v_g \approx 2\gamma \mu_0 M_s (D/\hbar) k$. As the micromagnetic group velocity is linear, it quickly diverges from the true group velocity, and thus the energy across the system dissipates faster as the wave number increases. This issue is apparent from the evolution of the spatially averaged magnetization along the z -axis, $\langle m_z \rangle$, shown in Fig. 5. The ASD results shown by hollow black circles are obtained from the same simulation presented in Fig. 4. The evolution using the micromagnetic approximation, shown by a red curve, is qualitatively different, with $\langle m_z \rangle$ displaying a faster relaxation towards equilibrium in the temporal range between ≈ 0.5 and 1 ps, and later showing a much slower relaxation until the end of the simulation at 500 ps. This is a consequence of the disparate group

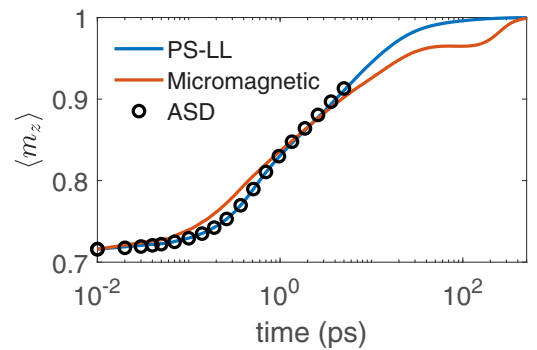


FIG. 5. Evolution of the average out-of-plane magnetization, $\langle m_z \rangle$, across the 1D ferromagnetic nanowire, generated from the same data set as Fig. 4. The results from PS-LL, the micromagnetic approximation, and ASD are shown by a solid blue curve, a solid red curve, and hollow black circles, respectively. The PS-LL and its micromagnetic approximation were run for 500 ps, until the magnetization reached equilibrium. The time is shown in natural logarithmic scale.

velocities between ASD and the micromagnetic approximation. In contrast, the PS-LL shown by a solid blue curve follows the ASD evolution accurately and then smoothly stabilizes to full saturation, converging to the micromagnetic description. We note that the same discrepancy in group velocities is observed in the context of MI. Examples of such an evolution are shown in the Supplemental Material SI 7 [45].

The presented results on the dynamic magnetization due to transient grating demonstrate that the PS-LL captures the main dynamical features due to exchange interaction. Further improvements can be achieved by including thermal fluctuations. For example, the ASD model takes into account light-matter interaction via the two-temperatures model, in which the electronic and spin systems are coupled. An example calculation of the spin temperature and magnetization evolution is shown in the Supplemental Material SI 8 [45]. Because of the lingering temperature in the ASD model, the magnetization evolution is not quantitatively reproduced by PS-LL. However, the two-temperatures model calculation could be included in the PS-LL model in parallel with the evolution of the magnetization dynamics. Similar to ASD, the addition of a random fluctuation term would require a stiffer solver, e.g., a Heun method. It would also be interesting to take advantage of the multiscale properties afforded by the PS-LL to explore a smooth-scale transition based on the Landau-Lifshitz-Bloch equation and

respecting the correct rescaling of the magnetization vector, e.g., Ref. [25].

In summary, we have introduced the PS-LL as a continuum model that captures the relevant physics of atomic scale magnetism by dispersion engineering. This approach relies on the knowledge of the dispersion relation of magnons, and so it can be generalized to higher dimensions, other magnetic orders, and arbitrary exchange integral between spins in a multilattice material. In the context of ultrafast magnetism, excellent agreement with ASD suggests that the PS-LL can resolve the multiscale evolution of the magnetization without incurring violation of energy and momentum conservation. The PS-LL will be valuable to provide both analytical and numerical insights into the short-time evolution of far-from-equilibrium magnetization, including the onset and evolution of topological defects [11,29].

This work was supported by the U.S. Department of Energy, Office of Basic Energy Sciences under Award No. DE-SC-0024339. The ASD simulations were completed using resources provided by the Baskerville Tier 2 HPC service. Baskerville was funded by the EPSRC and UKRI through the World Class Labs scheme (EP/T022221/1) and the Digital Research Infrastructure Programme (EP/W032244/1), and it is operated by Advanced Research Computing at the University of Birmingham.

-
- [1] E. J. Sie *et al.*, An ultrafast symmetry switch in a Weyl semimetal, *Nature (London)* **565**, 61 (2019).
- [2] M. Budden, T. Gebert, M. Buzzi, G. Jotzu, E. Wang, T. Matsuyama, G. Meier, Y. Laplace, D. Pontiroli, M. Ricc , F. Schlawin, D. Jaksch, and A. Cavalleri, Evidence for metastable photo-induced superconductivity in K_3C_{60} , *Nat. Phys.* **17**, 611 (2021).
- [3] F. Zhou, J. Williams, S. Sun, C. D. Malliakas, M. G. Kanatzidis, A. F. Kemper, and C.-Y. Ruan, Nonequilibrium dynamics of spontaneous symmetry breaking into a hidden state of charge-density wave, *Nat. Commun.* **12**, 566 (2021).
- [4] I. Žutić, J. Fabian, and S. Das Sarma, Spintronics: Fundamentals and applications, *Rev. Mod. Phys.* **76**, 323 (2004).
- [5] A. Kirilyuk, A. V. Kimel, and T. Rasing, Ultrafast optical manipulation of magnetic order, *Rev. Mod. Phys.* **82**, 2731 (2010).
- [6] A. Kosevich, B. Ivanov, and A. Kovalev, Magnetic solitons, *Phys. Rep.* **194**, 117 (1990).
- [7] C. Donnelly, M. Guizar-Sicairos, V. Scagnoli, S. Gliga, M. Holler, J. Raabe, and L. J. Heyderman, Three-dimensional magnetization structures revealed with X-ray vector nanotomography, *Nature (London)* **547**, 328 (2017).
- [8] C. Donnelly, S. Finizio, S. Gliga, M. Holler, A. Hrabec, M. Odstrčil, S. Mayr, V. Scagnoli, L. J. Heyderman, M. Guizar-Sicairos, and J. Raabe, Time-resolved imaging of three-dimensional magnetization dynamics, *Nat. Nanotechnol.* **15**, 356 (2020).
- [9] C. Donnelly, K. L. Metlov, V. Scagnoli, M. Guizar-Sicairos, M. Holler, S. Bingham, N. J. Raabe, L. J. Heyderman, N. R. Cooper, and S. Gliga, Experimental observation of vortex rings in a bulk magnet, *Nat. Phys.* **17**, 316 (2021).
- [10] D. Turenne *et al.*, Nonequilibrium sub-10 nm spin-wave soliton formation in FePt nanoparticles, *Sci. Adv.* **8**, eabn0523 (2022).
- [11] A. Rana *et al.*, Three-dimensional topological magnetic monopoles and their interactions in a ferromagnetic metal lattice, *Nat. Nanotechnol.* **18**, 227 (2023).
- [12] M. Di P. Mart nez, A. Wartelle, C. H. Mart nez, F. Fetta, F. Blondelle, J.-F. Motte, C. Donnelly, L. Turnbull, F. Ogrin, G. van der Laan, H. Popescu, N. Jaouen, F. Yakhou-Harris, and G. Beutier, Three-dimensional tomographic imaging of the magnetization vector field using fourier transform holography, *Phys. Rev. B* **107**, 094425 (2023).
- [13] B. Pfa, *et al.*, Ultrafast optical demagnetization manipulates nanoscale spin structure in domain walls, *Nat. Commun.* **3**, 1100 (2012).
- [14] D. Zusin *et al.*, Ultrafast perturbation of magnetic domains by optical pumping in a ferromagnetic multilayer, *Phys. Rev. B* **106**, 144422 (2022).
- [15] N. Z. Hagstr m *et al.*, Symmetry-dependent ultrafast manipulation of nanoscale magnetic domains, *Phys. Rev. B* **106**, 224424 (2022).
- [16] R. Jangid, N. Z. Hagstr m, M. Madhavi, K. Rockwell, J. M. Shaw, J. A. Brock, M. Pancaldi, D. De Angelis, F. Capotondi, E. Pedersoli, H. T. Nembach, M. W. Keller, S. Bonetti, E. E. Fullerton, E. Iacocca, R. Kukreja, and T. J. Silva, Extreme domain wall speeds under ultrafast optical excitation, *Phys. Rev. Lett.* **131**, 256702 (2023).
- [17] E. Iacocca *et al.*, Spin-current-mediated rapid magnon localization and coalescence after ultrafast optical pumping of ferrimagnetic alloys, *Nat. Commun.* **10**, 1756 (2019).

- [18] F. Büttner *et al.*, Observation of fluctuation-mediated picosecond nucleation of a topological phase, *Nat. Mater.* **20**, 30 (2021).
- [19] C. Andreas, A. Kákay, and R. Hertel, Multiscale and multi-model simulation of Bloch-point dynamics, *Phys. Rev. B* **89**, 134403 (2014).
- [20] R. F. L. Evans, D. Hinzke, U. Atxitia, U. Nowak, R. W. Chantrell, and O. Chubykalo-Fesenko, Stochastic form of the Landau-Lifshitz-Bloch equation, *Phys. Rev. B* **85**, 014433 (2012).
- [21] R. F. L. Evans, W. J. Fan, P. Chureemart, T. A. Ostler, M. A. A. Allis, and R. W. Chantrell, Atomistic spin model simulations of magnetic nanomaterials, *J. Phys.: Condens. Matter* **26**, 103202 (2014).
- [22] T. A. Ostler, R. F. L. Evans, R. W. Chantrell, U. Atxitia, O. Chubykalo-Fesenko, I. Radu, R. Abrudan, F. Radu, A. Tsukamoto, A. Itoh, A. Kirilyuk, T. Rasing, and A. Kimel, Crystallographically amorphous ferrimagnetic alloys: Comparing a localized atomistic spin model with experiments, *Phys. Rev. B* **84**, 024407 (2011).
- [23] J. Barker and G. E. W. Bauer, Semiquantum thermodynamics of complex ferrimagnets, *Phys. Rev. B* **100**, 140401(R) (2019).
- [24] A. Kartsev, M. Augustin, R. F. L. Evans, K. S. Novoselov, and E. J. G. Santos, Biquadratic exchange interactions in two-dimensional magnets, *npj Comput. Mater.* **6**, 150 (2020).
- [25] F. Jakobs and U. Atxitia, Bridging atomistic spin dynamics methods and phenomenological models of single-pulse ultrafast switching in ferrimagnets, *Phys. Rev. B* **106**, 134414 (2022).
- [26] W. F. Brown, *Micromagnetics* (Interscience, Huntington, NY, 1963).
- [27] C. Abert, Micromagnetics and spintronics: models and numerical methods, *Eur. Phys. J. B* **92**, 120 (2019).
- [28] M. Krawczyk, M. L. Sokolovskyy, J. W. Klos, and S. Mamica, On the formulation of the exchange field in the Landau-Lifshitz equation for spin-wave calculation in magnonic crystals, *Adv. Condens. Matter Phys.* **2012**, 764783 (2012).
- [29] R. Balakrishnan, R. Dandoloﬀ, and A. Saxena, Exact hopfion vortices in a 3D Heisenberg ferromagnet, *Phys. Lett. A* **480**, 128975 (2023).
- [30] U. Atxitia, D. Hinzke, O. Chubykalo-Fesenko, U. Nowak, H. Kachkachi, O. N. Mryasov, R. F. Evans, and R. W. Chantrell, Multiscale modeling of magnetic materials: Temperature dependence of the exchange stiffness, *Phys. Rev. B* **82**, 134440 (2010).
- [31] E. Méndez, M. Poluektov, G. Kreiss, O. Eriksson, and M. Pereiro, Multiscale approach for magnetization dynamics: unraveling exotic magnetic states of matter, *Phys. Rev. Res.* **2**, 013092 (2020).
- [32] D. Arjmand, M. Poluektov, and G. Kreiss, Modelling long-range interactions in multiscale simulations of ferromagnetic materials, *Adv. Comput. Math.* **46**, 2 (2020).
- [33] G. B. Whitham, *Linear and Nonlinear Waves* (Wiley, 1974).
- [34] V. Zakharov and L. Ostrovsky, Modulation instability: The beginning, *Physica D* **238**, 540 (2009).
- [35] E. B. Sonin, Spin currents and spin superfluidity, *Adv. Phys.* **59**, 181 (2010).
- [36] S. Takei and Y. Tserkovnyak, Superfluid spin transport through easy-plane ferromagnetic insulators, *Phys. Rev. Lett.* **112**, 227201 (2014).
- [37] E. Iacocca, T. J. Silva, and M. A. Hofer, Breaking of Galilean invariance in the hydrodynamic formulation of ferromagnetic thin films, *Phys. Rev. Lett.* **118**, 017203 (2017).
- [38] E. Iacocca and M. A. Hofer, Perspectives on spin hydrodynamics in ferromagnetic materials, *Phys. Lett. A* **383**, 125858 (2019).
- [39] F. Bencivenga *et al.*, Nanoscale transient gratings excited and probed by extreme ultraviolet femtosecond pulses, *Sci. Adv.* **5**, eaaw5805 (2019).
- [40] K. R. Rouxel *et al.*, Hard X-ray transient grating spectroscopy on bismuth germanate, *Nat. Photon.* **15**, 499 (2021).
- [41] D. Ksenzov, A. A. Maznev, V. Unnikandanunni, F. Bencivenga, F. Capotondi, A. Caretta, L. Foglia, C. Malvestuto, M. Masciovecchio, R. Mincigrucci, K. A. Nelson, M. Pancaldi, E. Pedersoli, L. Randolph, H. Rahmann, S. Urazhdin, S. Bonetti, and C. Gutt, Nanoscale transient magnetization gratings created and probed by femtosecond extreme ultraviolet pulses, *Nano Lett.* **21**, 2905 (2021).
- [42] L. Foglia *et al.*, Extreme ultraviolet transient gratings: A tool for nanoscale photoacoustics, *Photoacoustics* **29**, 100453 (2023).
- [43] F. Bencivenga, F. Capotondi, L. Foglia, R. Mincigrucci, and C. Masciovecchio, Extreme ultraviolet transient gratings, *Adv. Phys.: X* **8**, 2220363 (2023).
- [44] J. D. Carter, Bidirectional whitham equations as models of waves on shallow water, *Wave Motion* **82**, 51 (2018).
- [45] See Supplemental Material at <http://link.aps.org/supplemental/10.1103/PhysRevB.109.L180404> for the derivation of the dispersion relation of a 1D ferromagnetic chain in the PS-LL model, reproduction of the dispersion relation past the FBZ, derivation of the general spin hydrodynamic equations, setup for the atomistic spin dynamic simulations, micromagnetic approximation within the PS-LL model, results for transient gratings with different periodicities, onset of modulational instability due to transient grating, and simulations using atomistic spin dynamics to predict the magnetization distribution due to transient grating from a laser pulse.
- [46] G. A. El and M. A. Hofer, Dispersive shock waves and modulation theory, *Physica D* **333**, 11 (2016).